Momentum corrections for E1-6 using kinematical fits

F. Sabatié
CEA Saclay, DAPNIA/SPhN
Email: *sabatie@jlab.org*

July 21, 2003

Abstract

A general purpose electroproduction kinematical fit library has been developed and applied to momentum corrections for the E1-6 run period. Using $ep \to e\pi^+(n)$ and/or $ep \to ep(\gamma)$ radiative elastic events, we have extracted momentum corrections for electrons and π^+ as a function of their momentum, azimuthal and polar angles. The corrections being rather small for the E1-6 run period, this procedure does not give much better results than the momentum-independent method using elastic scattering. However, it is much more general and can be be applied to all kinds of processes and data if the statistics is sufficient.

1 Introduction

Due to limitations or imperfections in the knowledge of the magnetic field and of the position of drift chambers, momentum corrections have to be applied to CLAS data, especially to electron runs. In previous experiments such as E1, momentum corrections as high as a few percents have been derived using essentially two methods: the first method used the over-constrained elastic scattering process. Only the proton angle was assumed to be correct, the other variables were all deduced from this and momentum corrections as a function of polar and azimuthal angles were deduced. The main drawback of such a method is the very limited phase space covered by elastic scattering. Moreover, the underlying assumption that the momentum corrections are independent of the particle momentum is not justified. The second method uses the radiative elastic process where a photon is emitted close to 0° and goes undetected inside the beam pipe. The kinematics is still over-constrained. The assumption in this case is that both the electron and proton angles are reconstructed correctly. One can therefore have a momentum correction as a function of momentum and angles.

The procedure used in this work is a generalization of the second method described in the previous paragraph. The principle is very simple: all well identified over-constrained reactions can be used to correct all measured particles momenta and angles. First, one performs a kinematical fit on the identified reaction. Differences between the measured and fitted variable can be histogrammed in different bins of momentum, angles, sectors and of course particle type (especially charge). These histograms are then fitted to gaussians + background and put into tables. The mean value of the gaussian is used for momentum correction.

After explaining the kinematical fit procedure, we will show how momentum corrections were derived using this method. Results and issues will be explained next. The fifth section consists in a howto guide to this C++ momentum correction class for everyone to use. Finally, some conclusions will be drawn.

2 Kinematical fit procedure

Kinematical fits (least-square estimation with constraints) have been performed for a long time and the procedure is well known. As a reference, we will write down the equations used in our implementation

of this method.

The problem is the following: a certain channel is well identified through the measurement of N variables. Energy-momentum conservation law and possibly other constraints (invariant masses equal to some particle's mass and so on) add up into a set of K constraint equations. Possibly, some particles are not detected or more generally some variables are not measured and we end up with J unmeasured variables.

A least square estimation will basically investigate the kinematic hypothesis; for a successful minimization the constraint equations will supply estimates for the unmeasured variables as well as "improved measurements" for the measured quantities. The momentum corrections will be extracted from these "improved measurements".

2.1 The iteration procedure

Let us define $\vec{\eta}$ as the column vector of N measured quantities (typically includes momenta and angles). The column vector $\vec{y}$ is the first approximation (or measurements), with their errors contained in the covariance matrix $\mathbf{V}(\vec{y})$ (dimension $N \times N$). In addition, we have a set of J unmeasured variables contained in the $\vec{\xi}$ column vector. The N measured and J unmeasured variables are related and have to satisfy a set of K constraint equations f_k which can be written as:

$$f_k(\vec{\eta}, \vec{\xi}) = 0 \ , \quad \text{for } k = 1, ..., K \ . \tag{1}$$

According to the least square principle, the best estimate of the unknowns $\vec{\eta}$ and $\vec{\xi}$ are achieved for the following conditions:

$$\left\{ \begin{array}{lcl} \chi^2(\vec{\eta}) & = & (\vec{y} - \vec{\eta})^T \mathbf{V}^{-1}(\vec{y})(\vec{y} - \vec{\eta}) = \text{minimum} \\ \vec{f}(\vec{\eta}, \vec{\xi}) & = & \vec{0} \ . \end{array} \right. \tag{2}$$

The method of Lagrange multipliers is used to deal with the K constraint equations in the minimization procedure. Let us introduce K additional unknowns which can be written in the form of a column vector $\vec{\lambda}$. We can rephrase the problem and require:

$$\chi^2(\vec{\eta}, \vec{\xi}, \vec{\lambda}) = (\vec{y} - \vec{\eta})^T \mathbf{V}^{-1}(\vec{y})(\vec{y} - \vec{\eta}) + 2\vec{\lambda}^T \vec{f}(\vec{\eta}, \vec{\xi}) = \text{minimum} \ . \tag{3}$$

The number of unknowns is now $N + J + K$. The minimum is achieved by requiring the derivatives of χ^2 with respect to all unknowns equal to zero. After some algebra, one obtains the following set of equations:

$$\left\{ \begin{array}{lcll} \vec{\nabla}_\eta \chi^2 & = & -2\mathbf{V}^{-1}(\vec{y} - \vec{\eta}) + 2\vec{F}_\eta^T \lambda = \vec{0} & (N \quad \text{equations}) \\ \vec{\nabla}_\xi \chi^2 & = & 2\mathbf{F}_\xi^T \lambda = \vec{0} & (J \quad \text{equations}) \\ \vec{\nabla}_\lambda \chi^2 & = & 2\vec{f}(\vec{\eta}, \vec{\xi}) = \vec{0} & (K \quad \text{equations}) \ , \end{array} \right. \tag{4}$$

where the matrices $\mathbf{F}_\eta$ (of dimension $K \times N$) and $\mathbf{F}_\xi$ (of dimension $K \times J$) are defined by:

$$(F_\eta)_{ki} \equiv \frac{\partial f_k}{\partial \eta_i} \ , \qquad (F_\xi)_{kj} \equiv \frac{\partial f_k}{\partial \xi_j} \ . \tag{5}$$

The result from the set of $N + J + K$ equations will be solved using an iterative procedure, producing successively better approximations. The actual method uses a Taylor expansion of the constraint equations around the result of the current iteration. Taking only the first order is enough to get a convergence in a few iterations at most, which is a requirement for a relatively fast algorithm. Let us place ourselves after iteration number ν has been performed. We have approximations for all $N + J + K$ variables contained in vectors $\vec{\eta}^\nu$, $\vec{\xi}^\nu$ and $\vec{\lambda}^\nu$. After linearization of the constraint equations and some semi-painful algebra, the values of the same variables at the next iteration $\nu + 1$ are given by:

$$\left\{ \begin{array}{lcl} \vec{\xi}^{\nu+1} & = & \vec{\xi}^\nu - \left(\mathbf{F}_\xi^T \mathbf{S} \mathbf{F}_\xi \right)^{-1} \mathbf{F}_\xi^T \mathbf{S}^{-1} \vec{r} \\ \vec{\lambda}^{\nu+1} & = & \mathbf{S}^{-1} \left[\vec{r} + \mathbf{F}_\xi \left(\vec{\xi}^{\nu+1} - \vec{\xi}^\nu \right) \right] \\ \vec{\eta}^{\nu+1} & = & \vec{y} - \mathbf{V} \mathbf{F}_\eta^T \vec{\lambda}^{\nu+1} \ , \end{array} \right. \tag{6}$$

where the column vector $\vec{r}$ and matrix $\mathbf{S}$ (symmetric matrix of dimension $K \times K$) are given by the following relations:

$$\vec{r} = \vec{f}^{\nu} + \mathbf{F}_{\eta}^{\nu}(\vec{y} - \vec{\eta}^{\nu}) \ , \tag{7}$$

$$\mathbf{S} = \mathbf{F}_{\eta}^{\nu}\mathbf{V}(\mathbf{F}_{\eta}^{\nu})^{T} \ . \tag{8}$$

Note that the matrices $\mathbf{F}_{\eta}$, $\mathbf{F}_{\xi}$, $\mathbf{S}$ and vector $\vec{r}$ are evaluated at the point $(\vec{\eta}^{\nu}, \vec{\xi}^{\nu})$. The next step consists in calculating the new χ^2:

$$(\chi^2)^{\nu+1} = (\vec{\lambda}^{\nu+1})^{T}\mathbf{S}\vec{\lambda}^{\nu} + 2(\vec{\lambda}^{\nu+1})^{T}\vec{f}^{\nu+1} \ . \tag{9}$$

The procedure is repeated until the χ^2 becomes "small enough". For our case, we have iterated until the difference of χ^2 between one iteration and the next was smaller than 0.001, which was achieved in 2 to 3 iterations for most events.

2.2 Covariance matrix calculation

The CLAS software tracking errors are unreliable[1] and do not reflect the systematic errors which momentum corrections are trying to correct for. Therefore, we have chosen to use a fully diagonal covariance matrix. The momenta and angles' errors/resolutions are derived from fits which can be found in the CLAS NIM [1]. This study was performed at a fixed polar angle equal to 35°, but large angular dependence have been derived from past momentum corrections studies. Therefore, we have improved the CLAS NIM formula with another term which depends on θ to match the increase in systematic errors at small angle. The momentum and angular resolution formulae we have used are the following:

$$\begin{cases} \text{if } \theta < 41.93^{\circ} \quad \text{then} \quad \sigma_p = \frac{3375}{I_{\text{torus}}} \cdot \sqrt{0.0033^2 \cdot p^2 + 0.002^2 \cdot A^2(\theta) + (0.0018/\beta)^2} \\ \qquad\qquad\qquad\qquad \text{with } A(\theta) = 10.8254 - 0.395191 \cdot \theta + 0.00326775 \cdot \theta^2 \\ \text{if } \theta \geq 41.93^{\circ} \quad \text{then} \quad \sigma_p = \frac{3375}{I_{\text{torus}}} \cdot (0.0018/\beta) \ , \end{cases} \tag{10}$$

$$\sigma_{\theta} = \sqrt{0.00055^2 + \left(\frac{0.00139}{p \cdot \beta}\right)^2} \quad , \tag{11}$$

$$\sigma_{\phi} = \sqrt{0.00373^2 + \left(\frac{0.00314}{p \cdot \beta}\right)^2} \quad . \tag{12}$$

Tests with a much cruder description of momentum and angular resolutions were tested and no strong sensitivity of the final result to the description resolutions were found.

3 Extraction of momentum corrections

In order to have a meaningful result, the momentum correction tables have to contain enough bins in θ, ϕ and p (for each particle type and each sector). The main limitation of the momentum correction method described in this note is the statistical significance of the result. In order to have a reasonable phase space coverage, one has to choose processes for which there is a large data sample in the E1-6 data. Two such processes have been found: $ep \rightarrow e\pi^{+}(n)$ and $ep \rightarrow ep(\gamma)$ where the γ is emitted close to 0° (radiative tail of elastic scattering). The identification of both processes is rather straightforward and there is little contamination by other channels. Moreover, our event selection is rather drastic to avoid excessive contamination. One should note that the $(en\pi^{+})$ data sample allows the simultaneous correction of both the electron and positive pion, which is useful for the processes of interest of the Saclay group in E1-6: the ω and ρ electroproductions.

[1] If someone could tell me if this is just a legend or if it is not, why this is the case, I would be most grateful.

Figure 1 shows the phase space in θ vs. p covered by the electrons in the $ep \to en\pi^+$, $ep \to ep\gamma$ and elastic processes[2]. One can see that although the relative weights in the phase space is different for the two first processes, the coverage is much larger than in the elastic case. Actually, the coverage for $(en\pi^+)$ and $(ep\gamma)$ are rather complementary. The former reaction has much more events at large electron momentum, whereas the latter is concentrated at small electron momentum. The binning chosen for the momentum correction extraction is listed at the end of this section.

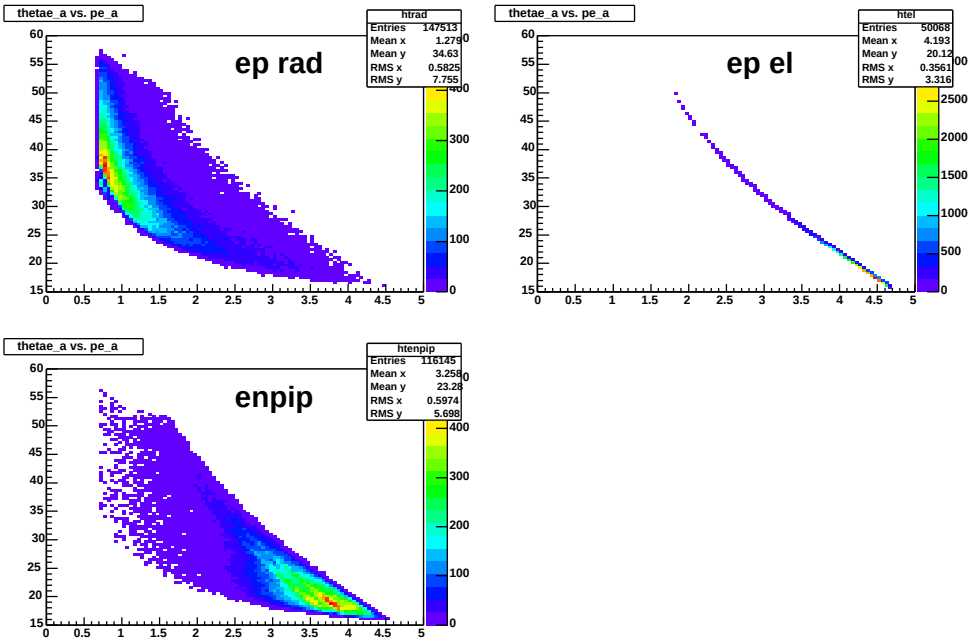

Figure 1: Phase space in θ vs. p covered by the electrons in the $ep \to en\pi^+$, $ep \to ep\gamma$ and elastic processes.

Figure 2 shows an example of several fits of $p_{\rm corr}/p_{\rm meas}$ using (gaussian + background) performed for $25^\circ < \theta \leq 27^\circ$, $-5^\circ < \phi \leq 0^\circ$ for various bins in electron momentum, for the $(en\pi^+)$ sample. Figure 3 shows the ratio $p_{\rm corr}/p_{\rm meas}$ as a function of ϕ for different bins in θ integrated over p. Note that similar ϕ behaviors were extracted for all processes as well as for previous momentum correction studies [2, 3]. In addition, corrections using elastic data derived from kinematical fits are found to be consistent with the usual method used to deduce momentum corrections from elastic scattering [2].

The fits performed on the $(en\pi^+)$, $(ep\gamma)$ and elastic data can be compared in the region where data samples have enough events and overlap. For instance, Fig. 4 shows the momentum dependence of $p_{\rm corr}/p_{\rm meas}$ in the $25^\circ < \theta \leq 27^\circ$, $-5^\circ < \phi \leq 0^\circ$ bin. Note that the $(ep\gamma)$ and elastic data have had energy loss corrections applied to the proton whereas this was not necessary for the $(en\pi^+)$ sample. Some inconsistencies in the range of overlap of the $(ep\gamma)$ and $(en\pi^+)$ remain, for most of the phase space. The inconsistency has been investigated but no straightforward source was found. We conclude from the $en\pi^+/ep\gamma/ep$ comparison that systematic errors on the resulting corrections are of the order $1\text{-}2{\cdot}10^{-3}$. At this level of precision, even electron or pion energy loss should also be taken into account.

A better version of proton energy loss corrections [4] turned out to modify the quality of the $(ep\gamma)$ corrections. Therefore, we chose to use the $(en\pi^+)$ sample as a reference. Both options are available in the momentum correction class (see section 5). In addition, using the same process and method, we have extrated the momentum corrections for positive pions.

The bins in θ, ϕ and p used for the electron momentum corrections are the following (only edges):

[2]Note that in these figures as well as our whole momentum correction study, the "official" E1-6 fiducial cuts were applied to the data samples.

- θ_e : 15, 20, 25, 30, 35, 40, 45, (50, 55)
- ϕ_e : -18, -15, -12, -9, -6, -3, 0, 3, 6, 9, 12, 15, 18
- p_e : 0.7, 1.0, 1.3, 1.6, 1.9, 2.2, 2.5, 2.8, 3.1, 3.4, 3.7, 4.0, 4.3

For the $(en\pi^+)$ sample, only 6 bins in p_e from 15 to 45° were taken, whereas two extra bins were achievable for the $(ep\gamma)$ sample. The bins in θ, ϕ and p used for the π^+ momentum corrections are the following (only edges):

- θ_{π^+} : 10, 18, 26, 34, 42, 50, 58
- ϕ_{π^+} : -24, -20, -16, -12, -8, -4, 0, 4, 8, 12, 16, 20, 24
- p_{π^+} : 0.25, 0.50, 0.75, 1.00, 1.25, 1.50, 1.75, 2.00, 2.25, 2.50, 2.75, 3.00, 3.25

4 Performances

The performances of the momentum corrections were checked on the $ep \to ep\omega$ and $ep \to en\pi^+$ processes. For the ω electroproduction, we have selected events where one detects the positive pion out of the three-pion decay of the ω. Figure 5 shows the ω peak in the epX missing mass for the 6 sectors, before and after corrections. Figure 6 represents the same quantity as a function W. Overall, the mean values of the mass peaks tends to converge towards the right value and the width of the distributions improve by up to 20%. No W-dependence of the mass distributions is observed, before or after corrections. The summary of Fig. 5 in terms of mean and sigma of the mass distributions are shown in Table 1 below:

Sector	Before Corr.		After Corr.	
	M_ω	σ_{M_ω}	M_ω	σ_{M_ω}
1	0.788	0.013	0.783	0.013
2	0.781	0.011	0.781	0.010
3	0.782	0.012	0.782	0.010
4	0.787	0.012	0.783	0.011
5	0.791	0.012	0.784	0.010
6	0.786	0.014	0.783	0.012

Table 1: Summary of the means and sigmas of the gaussians fitted in Figure 5.

Performances were also checked on the $ep \to en\pi^+$ channel with both electron and pion momentum corrections. Figure 7 shows the missing mass $(e\pi^+X)$ before and after correction of both detected particles' momenta. Before correction, the neutron mass was shifted by up to 10 MeV. After correction, the neutron mass is around the right value at the 1-2 MeV level. The width of the distributions are also slightly improved after correction, by up to 20%. No W dependence before or after corrections is observed. Table 2 summarizes the results for this performance check. Note that we studied the performances using both the $(en\pi^+)$ and the $(ep\gamma)$ samples and even though both do a fairly decent job at correcting momenta, the results are slightly in favor of the $(en\pi^+)$ method.

5 How to use the TMomCorr C++ class

Momentum corrections have been imbeded into the TMomCorr C++ class, located in the CLAS `CVS` trunk, at `packages/clasroot/MomCorr`. After compilation, a shared library called `libROOTMomCorr.so` will be created in `$CLAS_SLIB`. In a program, one will have to include the corresponding header file: `#include "TMomCorr.h"` and link with the shared library.

The usage is the following: First, define one (global) `TMomCorr` object using either the default contructor, or the constructor with options. Two options are available:

Sector	Before Corr.		After Corr.	
	M_n	σ_{M_n}	M_n	σ_{M_n}
1	0.950	0.014	0.938	0.013
2	0.939	0.012	0.938	0.010
3	0.941	0.012	0.938	0.011
4	0.950	0.012	0.939	0.012
5	0.950	0.013	0.940	0.012
6	0.945	0.013	0.938	0.013

Table 2: Summary of the means and sigmas of the gaussians fitted in Figure 7.

- `TMomCorr momcorr_obj(0);` : Uses ($en\pi^+$) for electron momentum corrections (option 0, same as default constructor) ,
- `TMomCorr momcorr_obj(1);` : Uses ($ep\gamma$) for electron momentum corrections (option 1).

In all cases, one should use the following methods of the TMomCorr class for electron and π^+ case respectively to get the corrected momentum from the sector number, polar and azimuthal angles and momentum:

```
Float_t GetCorrMom_e(Int_t s, Float_t theta, Float_t p, Float_t phi),

Float_t GetCorrMom_pip(Int_t s, Float_t theta, Float_t p, Float_t phi),
```

where the `phi` variable stands for the azimuthal angle inside the sector, from -30 to 30°. All angles should be in degrees and the particle momentum should be in GeV/c. The function returns the corrected momentum, by looking into tables which are only loaded once at the construction of the `TMomCorr` object.

6 Conclusion

The E1-6 momentum corrections turned out to be 2 to 3 times smaller than for other runs, probably thanks to the straight track analysis and careful DC calibration [5]. However, they remain a necessity, not only to align sectors with respect to each other in order to perform global cuts, but also to correct for strong ϕ dependences at the edges of the acceptance or fiducial volumes.

The method proposed in this document covers a wide kinematical range. In principle, it could be further extended by taking some kind of weighted average of corrections coming from different reaction channels. This was not attempted because of some lack of consistency between the results of the considered channels.

We would like to thank D. Doré and L. Morand for their help in producing the data samples which were used to derive the momentum corrections , as well as M. Garçon for his advice during the course of this project. I would also like to thank M. Ito who helped me quite a bit to start things up with kinematical fits. Finally, the whole E1-6 collaboration helped me tremendously by commenting and criticizing this work at several meetings.

References

[1] B.A. Mecking *et al.*, Nucl. Inst. Meth. **A503** (2003) 513.

[2] K.J. Park, `http://www.jlab.org/~parkkj/index_pre.html`.

[3] S. Stepanyan *et al.*, CLAS Analysis note **01-006** (2001).

[4] S.A. Morrow, private communication.

[5] S.A. Morrow and M.D. Mestayer, CLAS note **02-010** (2002).

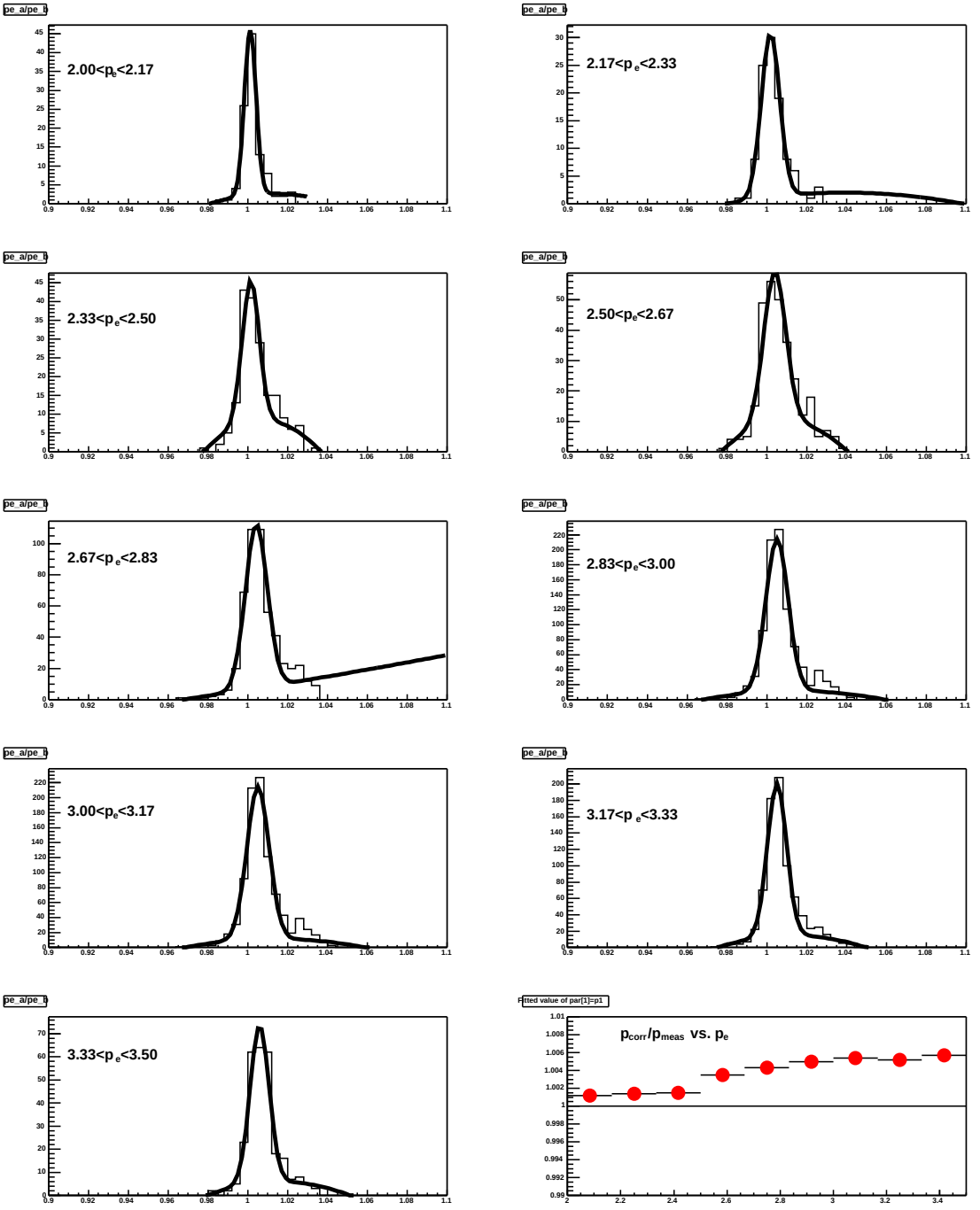

Figure 2: Example of several fits of $p_{\rm corr}/p_{\rm meas}$ using (gaussian + background) performed for $25^\circ < \theta \leq 27^\circ$, $-5^\circ < \phi \leq 0^\circ$ for various bins in electron momentum, for the reaction $en\pi^+$. The trend of increasing corrections towards larger momentum values is clear.

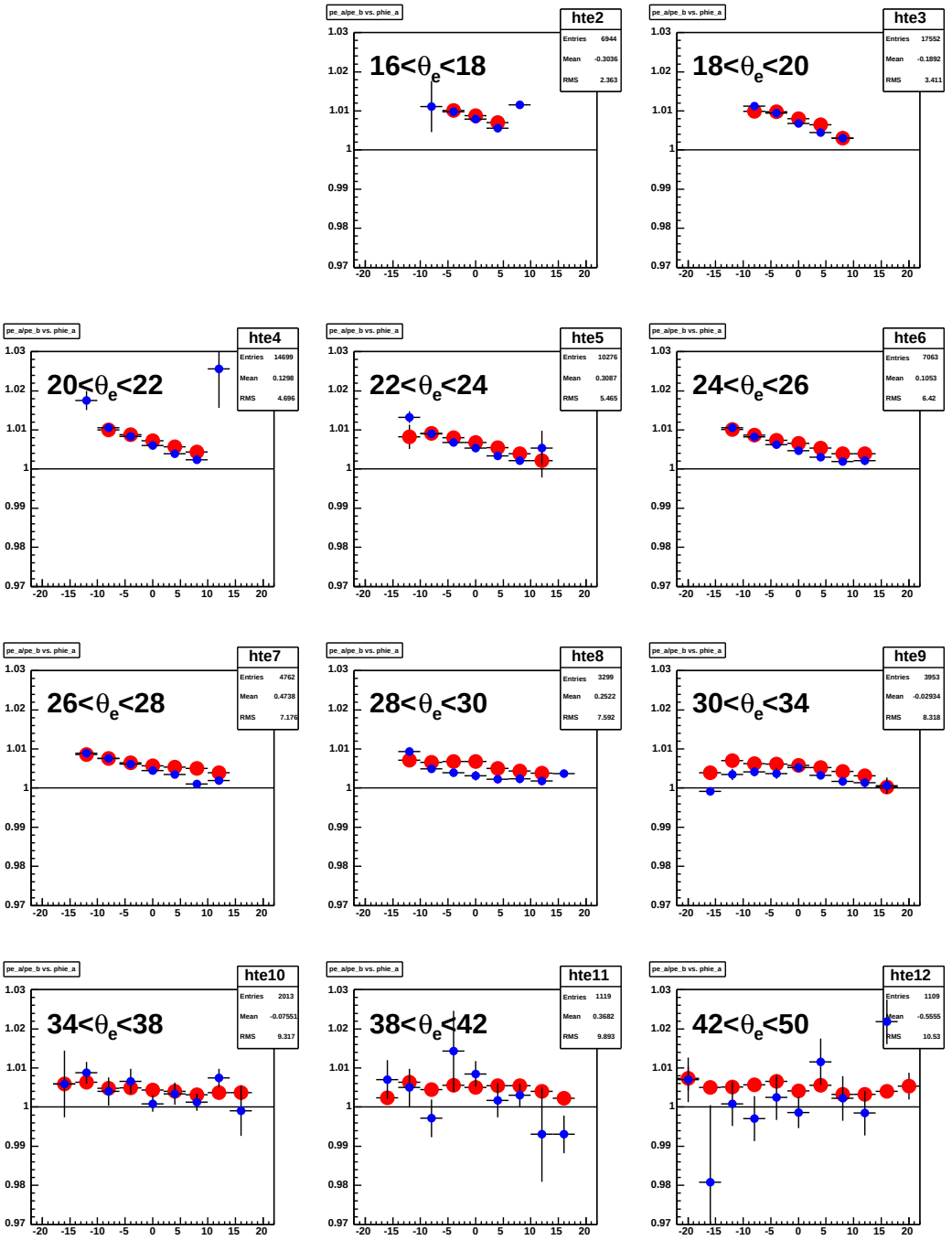

Figure 3: Azimuthal angle dependence of the ratio $p_{\rm corr}/p_{\rm meas}$ for different bins in θ and integrated over p. The big red circles correspond to the momentum corrections extracted from elastic data, the small blue circles correspond to the momentum corrections extracted from the $(en\pi^+)$ data sample. Since both data samples are integrated over the momentum, small differences in the ϕ behavior are expected. However, as mentioned before, electron momenta for the $ep \to en\pi^+$ tend to be large, rather close to the end point: the observed differences are small.

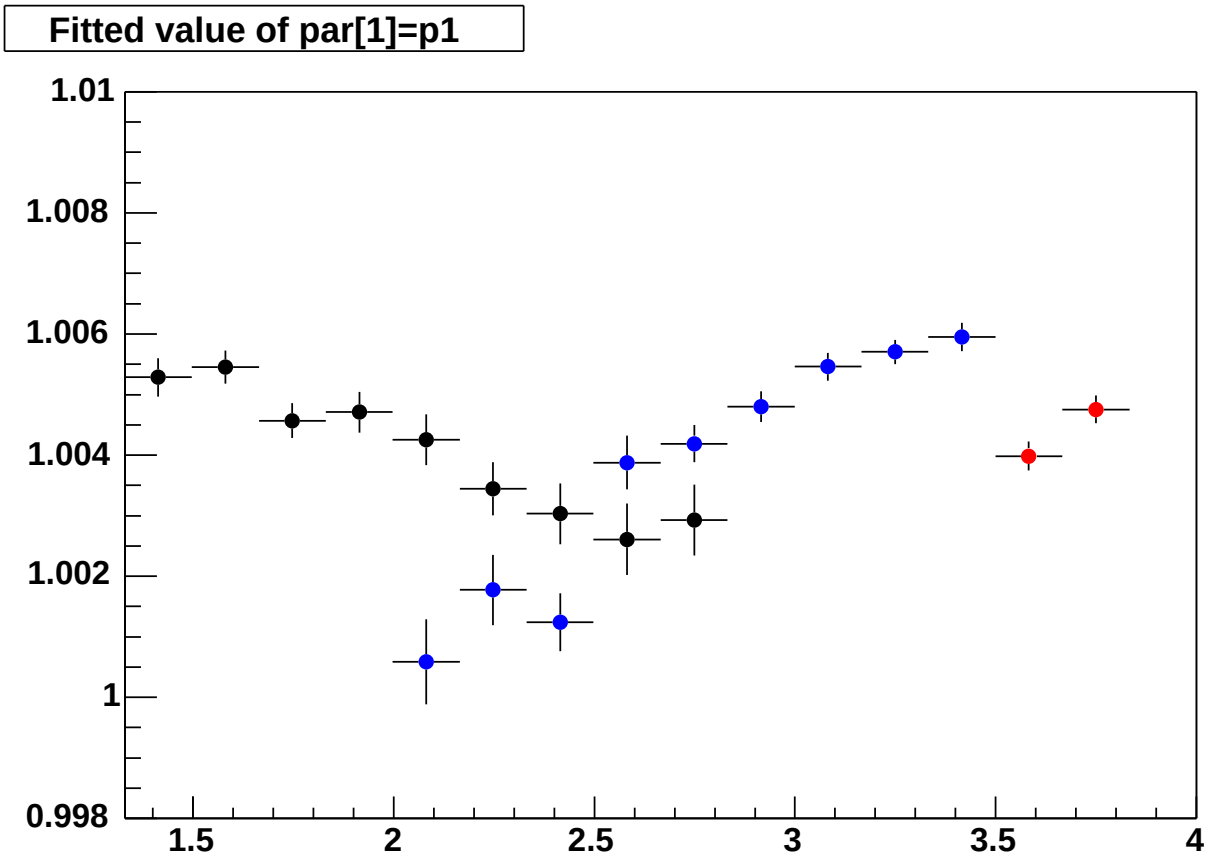

Figure 4: Comparisons of fits performed on the ($en\pi^+$) (blue), ($ep\gamma$) (black) and (ep) elastic (red) data samples, in the bin $25° < \theta \leq 27°$, $-5° < \phi \leq 0°$ bin, as function of electron momentum. Note that the ($ep\gamma$) and elastic data have had energy loss corrections applied to the proton whereas this was not necessary for the ($en\pi^+$) sample.

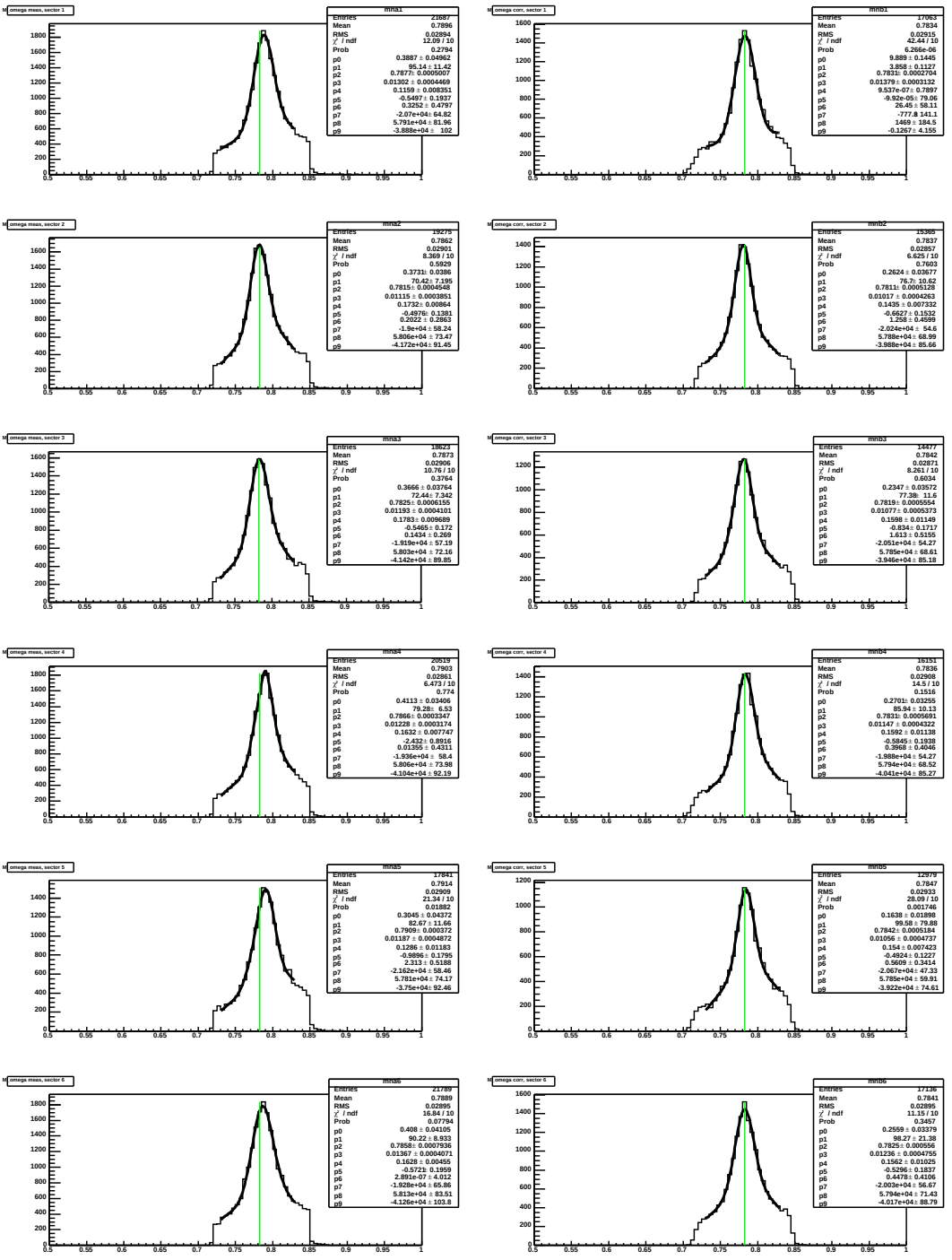

Figure 5: Missing mass (epX) showing the ω peak as a function of the sector in CLAS (sector 1 on top, 6 on the bottom) before electron momentum corrections (left plots) and after electron momentum corrections (right plots). A fit to a skewed gaussian + 2^{nd} order polynomial is adjusted to each histogram. Overall, the mean values converge towards the ω mass M_ω =0.783 GeV and the width of the distributions are improved by up to 20%, yielding a significant improvement.

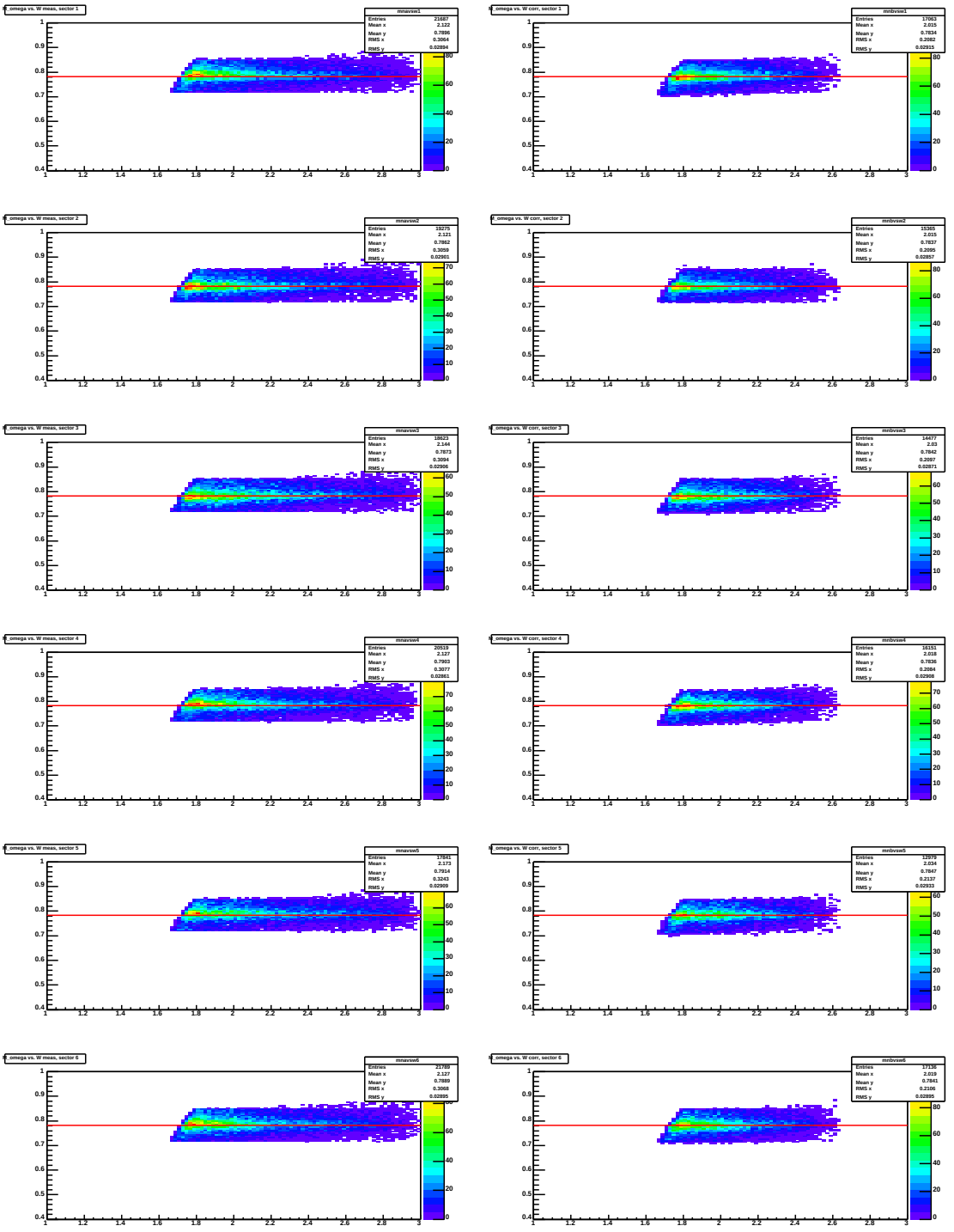

Figure 6: Missing mass (epX) as a function of W for the ω (sectors 1 to 6, top to bottom and before and after corrections, left and right plots). There were no striking W dependences of this observable as a function of W and there are still no dependence after corrections have been applied.

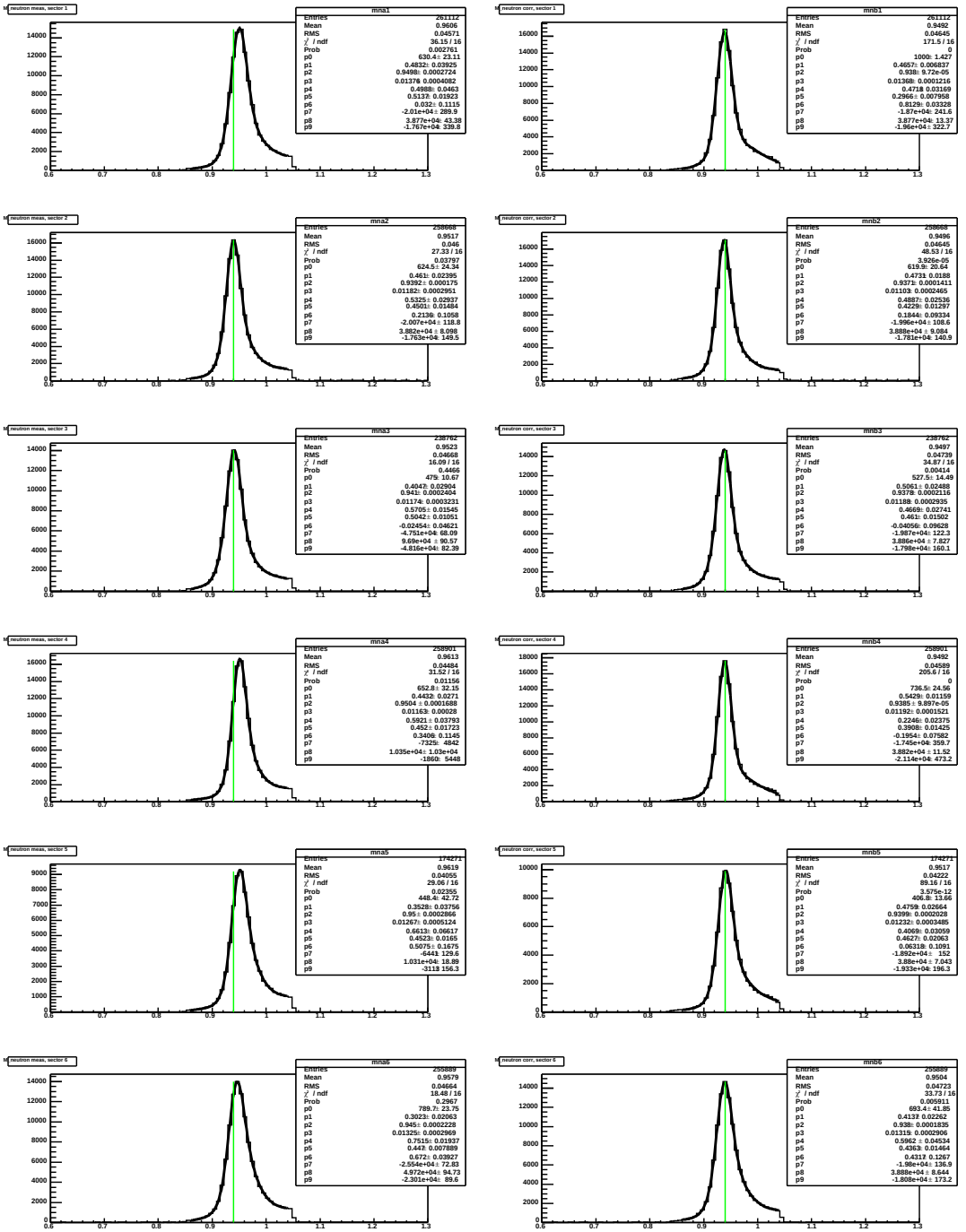

Figure 7: Missing mass ($e\pi^+X$) showing the neutron peak as a function of the sector in CLAS (sector 1 on top, 6 on the bottom) before electron and pion momentum corrections (left plots) and after corrections (right plots). A fit to a skewed gaussian + 2^{nd} order polynomial is adjusted to each histogram. Overall, the mean values converge towards the neutron mass and the width of the distributions are improved by up to 20%, yielding a significant improvement.